ANNALS OF TRANSPLANTATION

ORIGINAL PAPER

e-ISSN 2329-0358
© Ann Transplant, 2026; 31: e951930
DOI: 10.12659/AOT.951930

Received: 2025.10.28
Accepted: 2026.03.06
Available online: 2026.03.18
Published: 2026.XX.XX

Brain Death–Induced Systolic Ventricular Dysfunction and Its Association With NLRP3-Related Inflammatory Signaling in a Murine Model

Authors' Contribution:
Study Design A
Data Collection B
Statistical Analysis C
Data Interpretation D
Manuscript Preparation E
Literature Search F
Funds Collection G

ABCDEFG 1,2 Lei Huang
B 3 Kevin P. Zbierski
CD 2 Ye Yuan
CD 2 Siyuan Dong
C 3 Jacob Razzouk
ABCDEFG 3 David G. Rabkin

1 Department of Neurosurgery, Loma Linda University Medical Center, Loma Linda, CA, USA
2 Department of Physiology and Pharmacology, Loma Linda University School of Medicine, Loma Linda, CA, USA
3 Department of Cardiothoracic Surgery, Loma Linda University Medical Center, Loma Linda, CA, USA

Corresponding Author: David G. Rabkin, e-mail: drabkin@llu.edu
Financial support: This work was supported by a Grant for Collaborative and Translational Research (GCAT) award from the Loma Linda University School of Medicine
Conflict of interest: None declared

Background: Cardiac dysfunction after brain death limits donor heart utilization. We sought to define the incidence and time course of brain death (BD)–induced left ventricular (LV) dysfunction and its association with NLRP3-related inflammatory signaling in a murine model. Upstream regulators of NLRP3 signaling, including P2X7 and PPAR-γ, were also evaluated.

Material/Methods: Thirty C57BL/6 mice were studied. In phase I, mice were randomized to control (n=8) and BD (n=10) groups. Echocardiography was performed at baseline, and serially for 3 hours. Hemodynamic data were compared. In phase II, mice were randomized to control (n=6) and BD (n=6) groups. Similar measurements were obtained at baseline and periodically for 60 minutes (T60). Mice were killed, and LV tissue samples collected for biochemical analyses.

Results: In phase I, all BD animals developed significantly depressed LVEF by T60, with no deaths. Six animals in each group survived to T120, and 4 animals to T180. In phase II, all animals survived to T60. Mean LVEF, fractional shortening, and stroke volume were significantly reduced in the BD group. BD group demonstrated significantly greater expression of NLRP3, IL-1β, TNF-α, and IL-6 in LV tissue. P2X7 expression did not differ between groups, while PPAR-γ expression showed a trend toward increase in BD animals.

Conclusions: The incidence of depressed LV function was 100% at T60, with no attrition. BD-induced LV dysfunction was associated with increased expression of NLRP3 and pro-inflammatory cytokines in LV tissue, suggesting involvement of NLRP3-related inflammatory signaling. Targeting this pathway may represent a potential strategy to preserve myocardial function following brain death.

Keywords: Brain Death • Organ Preservation • Inflammation Mediators • Echocardiography

Abbreviations: **ATP** – adenosine triphosphate; **ANOVA** – analysis of variance; **BD** – brain death; **C57BL/6** – C57 Black 6; **IL** – interleukin; **LV** – left ventricular; **LVEF** – left ventricular ejection fraction; **NLRP3** – nucleotide-binding domain, leucine-rich-containing family and pyrin domain-containing protein 3; **P2X7** – purinergic P2X7 receptor 7; **PPAR-γ** – peroxisome proliferator-activated receptor gamma; **TNF** – tumor necrosis factor

Full-text PDF: https://www.annalsoftransplantation.com/abstract/index/idArt/951930

3935 3 5 27

Indexed in: [Science Citation Index Expanded] [Index Medicus/MEDLINE] [Chemical Abstracts] [Scopus]

Introduction

The greatest impediment to extending the gold-standard therapy of heart transplantation to tens of thousands of patients with end-stage heart failure is the shortage of available donor hearts. In the United States, approximately 20% of potential donors (roughly 1300 per year) are rejected exclusively due to poor cardiac function without structural abnormalities [1], likely the result of the pathophysiologic environment caused by the poorly understood phenomenon of brain death. Previous work has shown that carefully selected donor hearts with even advanced dysfunction can be transplanted with outcomes equivalent to that of donor hearts with normal function and that this dysfunction resolves over time [2,3]. However, utilization rates of donor hearts with poor function remain below 5% [1]. A method to demonstrate improvement in ventricular dysfunction in the brain-dead donor would be compelling evidence of the reversible nature of the cardiac dysfunction and may significantly increase utilization of this large pool of unused hearts. Understanding the mechanism by which brain death results in cardiac dysfunction is critical to furthering this goal. Therefore, to fill this gap in current clinical practice and move toward potential reversal strategies, we explored a potential mechanism using echocardiography to assess ventricular function simulating the standard clinical evaluation of potential donor hearts.

Brain death triggers an acute and massive release of catecholamines, resulting in an inflammatory state marked by significant proinflammatory cytokine upregulation, comparable to levels observed in sepsis [4]. This intense inflammatory cascade contributes to the impairment of donor heart contractile function [5]. Nucleotide-binding domain, leucine-rich-containing family and pyrin domain-containing protein 3 (NLRP3) belongs to the NOD-like receptor family [6]. NLRP3 signaling and inflammasome assembly are key regulators of inflammatory responses. A key involvement of the NLRP3 inflammasome has been reported across a variety of cardiovascular diseases [7,8]. However, the role of NLRP3-related inflammation in brain death–induced myocardial dysfunction has not been investigated.

Extracellular adenosine triphosphate (ATP) accumulates in inflammation and activates purinergic P2X7 receptor 7 (P2X7) in immune cells which in turn induces the formation of NLRP3 inflammasome, resulting in pyroptosis, an inflammatory type of cell death [9]. Specifically, NLRP3 inflammasome activation through heart-brain interaction upregulates myocardial interleukin (IL)-1β production by the ATP/P2X7 axis [10]. On the other hand, peroxisome proliferator–activated receptor gamma (PPAR-γ) is a nuclear receptor that functions as a transcription factor. It has been implicated as an endogenous modulator that attenuates NLRP3 inflammasome activation in macrophages [11]. Because P2X7 antagonists and PPAR-γ agonists are already commercially available [12,13], we chose to focus on this signaling pathway as a potentially modifiable link between brain death and cardiac dysfunction. Therefore, the present study aimed to first define the time course and incidence of brain death–induced left ventricular (LV) systolic dysfunction in a murine model and then to evaluate its association with NLRP3-related inflammatory signaling in LV tissue. We further examined expression of P2X7 and PPAR-γ, the upstream regulators of NLRP3, to explore potentially modifiable mechanisms linking brain death to myocardial inflammation.

Material and Methods

Ethics Statement

The study was approved by the Loma Linda University Institutional Animal Care and Use Committee (Institutional Animal Care and Use Committee Loma Linda University HEALTH, approval notice: IACUC 20-185: Elucidating mechanisms of brain death–induced cardiac dysfunction) and complied with the National Institutes of Health guidelines for the utilization of animals in research. All animals used in this study received proper care, use, and humane treatment in accordance with the Guide for the Care and Use of Laboratory Animals [14].

Experimental Model

Phase I

Eighteen 3-month-old C57 Black 6 (C57BL/6, Jackson laboratory, Farmington, CT, USA), specific pathogen-free, inbred mice were housed 2 to a cage and given free access to food and water with a standard 12-hour light/dark cycle. Anesthetic induction was accomplished with isoflurane (3-5%) until loss of consciousness and completion of the following: the animals were weighed, a depilatory cream was used on the chest, and they were placed supine on a heating pad with a heating lamp. Rectal temperature was recorded with a probe and an analog to digital converter. The electrocardiogram was sampled using needle-electrodes attached to the animals' extremities, at 200 Hz, with a single channel analog to digital converter (VisualSonics Vevo 2100 software) and recorded digitally. The electroencephalogram was sampled at 200 Hz with a 10-channel analog to digital converter (MP160 BIOPAC Systems Inc, Goleta, CA, USA) and recorded on a computer (MacBook; Apple Computer, Inc Cupertino, CA, USA). A tracheostomy was performed, and mice were connected to a small animal mechanical ventilator (RoVent Kent Scientific, Torrington, CT, USA), with a tidal volume of 150±25 µL, at a respiratory rate of 125 per minute. Respiratory rate, tidal volume, and peak inspiratory pressure were monitored in real time. Anesthesia was maintained

Indexed in: [Science Citation Index Expanded] [Index Medicus/MEDLINE] [Chemical Abstracts] [Scopus]

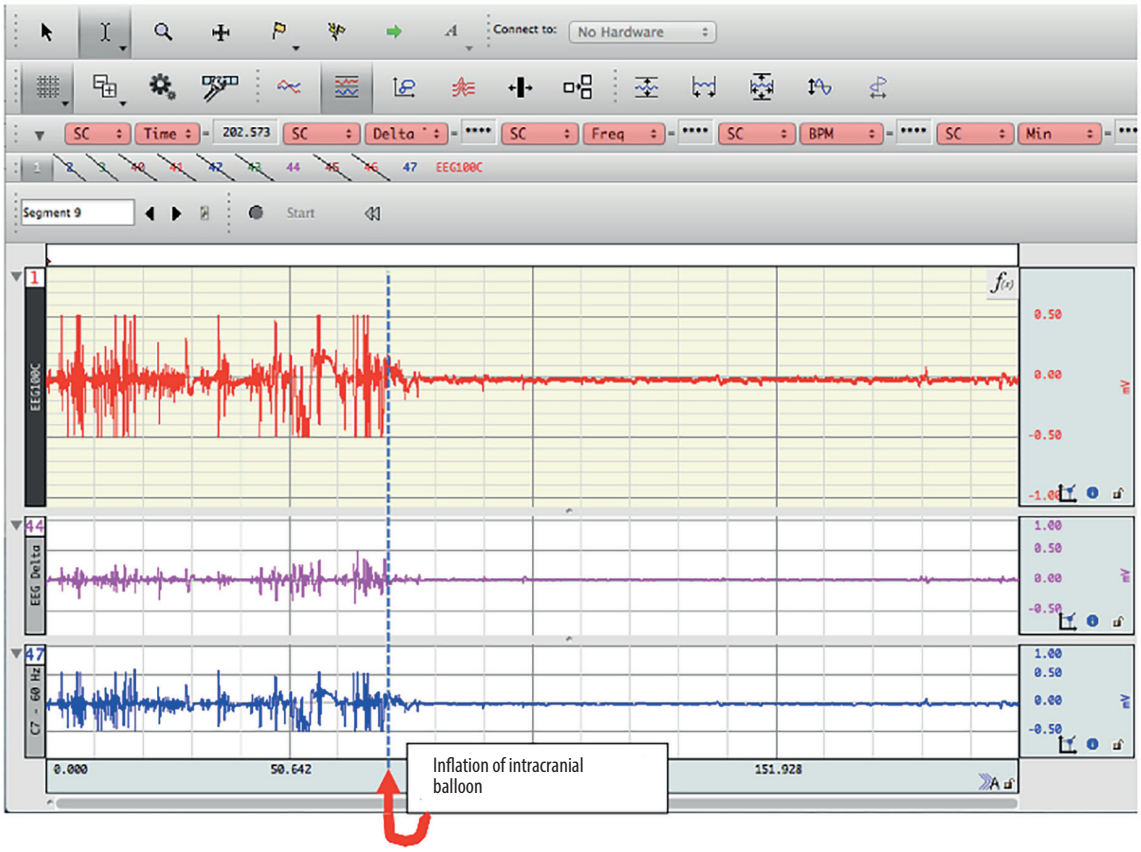

Figure 1. Representative electroencephalographic tracing during intracranial balloon inflation (red arrow).

with isoflurane (0.9-1%). Warm (35-36°C) lactated ringer's solution (0.5 mL) was injected subcutaneously between the shoulder blades or intraperitoneally every hour. Arterial blood gases were taken to assess the adequacy of gas exchange, as were a variety of laboratory values, including sodium, potassium, calcium, and glucose (Epocal, Inc, Ottawa, ON, Canada). After exposing the skull through an incision in the scalp, a burr hole was made in the cranium several millimeters lateral to the sagittal suture. A 2F micro-tip balloon catheter (0.15 mL) was inserted through the skull (Millar SP 407, Millar/ADInstruments, Colorado Springs, CO, USA) [15]. Animals were randomized to control or brain death (BD) groups by a flip of a coin. Control animals underwent identical surgical preparation, anesthesia, tracheostomy, ventilation, physiologic monitoring, and instrumentation, including burr hole creation and catheter placement, but without balloon inflation. This sham-instrumented control condition was chosen to isolate the physiologic effects of brain death from those related to anesthesia, mechanical ventilation, and surgical instrumentation.

For BD animals, brain death was induced with rapid inflation of the 0.15 mL balloon (<1 second), while control animals underwent the same procedure without balloon inflation. Brain death was determined by electroencephalographic quiescence with no electrical activity above 2 μV for 10 minutes (**Figure 1**) and confirmed by lack of corneal and oculocephalic reflexes. The anesthetic protocol was the same for both groups. Hemodynamic data were recorded, and echocardiography was performed (VisualSonics Vevo 2100, Bothell, WA, USA) in the parasternal long axis prior to induction of brain death (or sham procedure) at baseline, directly afterward (0 minute), at 15 and 30 minutes and then every half hour until 180 minutes had elapsed. The animals were then killed. We calculated hemodynamic data using the included software in the Cardiac Package with the parasternal long-axis protocol as follows. We traced the endocardium at diastole and systole in a cine loop (using the largest and smallest chamber sizes, respectively), allowing the software to interpolate between the traced contours to calculate the various cardiac parameters, including left ventricular ejection fraction (LVEF), fractional shortening, cardiac output, and stroke volume. After the measurements were calculated, we visually inspected the interpolated contours to ensure that the system had not inserted false values due to interpolation errors. We then exported the calculated data, along with the corresponding images, for further analysis.

Indexed in: [Science Citation Index Expanded] [Index Medicus/MEDLINE] [Chemical Abstracts] [Scopus]

Phase II

In the second phase of the experiment 12 C57BL/6 mice were also randomly divided into control (n=6) and BD (n=6) groups. They were instrumented in the same manner as phase I. Specifically, anesthetic induction and maintenance was accomplished with isoflurane (3-5% and 0.9-1%, respectively); temperature, electrocardiogram, and electroencephalogram were recorded in the same manner, and the animals were mechanically ventilated with a endotracheal tube placed through a tracheostomy. Both the control and BD animals underwent creation of a burr hole in the lateral cranium, and a micro-tipped balloon catheter was inserted, but only inflated for the BD group. Echocardiograms were performed and hemodynamic data recorded at baseline and times (T) 0, 15, 30, and 60 minutes after induction of BD or sham.

The mice were then killed, and LV samples were collected for the western blot assay of NLRP3, IL-1β, tumor necrosis factor (TNF)-α, IL-6, P2X7, and PPAR-γ expression. Western blot analysis assessed protein expression levels rather than direct functional assembly and catalytic activity of the inflammasome complex. Immediately after death, LV heart tissues were rapidly excised and placed in a dish on ice. Excess blood was gently rinsed off from the tissue with ice-cold phosphate buffered saline (2-3 times), after which LV heart tissues were transferred to pre-chilled microcentrifuge tubes, snap-frozen in liquid nitrogen, and stored at -80°C until further processing. For tissue homogenization, LV tissue from each animal was weighed and finely minced into small pieces using a clean, cold scalpel on a chilled surface. The tissue was then transferred to a pre-chilled homogenization tube, and ice-cold radioimmunoprecipitation assay lysis buffer (sc-24948, Santa Cruz Biotechnology, CA, USA) supplemented with protease and phosphatase inhibitors was added at a ratio of 500 µL per approximately 10 mg of tissue. Samples were thoroughly homogenized on ice using a mechanical tissue homogenizer, followed by incubation on ice for 30 minutes to ensure complete lysis. The homogenates were centrifuged at 14 000 rpm for 10 minutes at 4°C. The supernatant (whole-cell protein extract) was carefully transferred to a new pre-chilled microcentrifuge tube, and the protein concentration was determined using a detergent-compatible assay kit (Bio-Rad, Hercules, CA, USA).

For western blot assay, equal amounts of protein samples (30 µg) along with molecular marker were loaded onto 12% sodium dodecyl sulfate-polyacrylamide gel electrophoresis gels, separated by electrophoresis, and subsequently transferred onto nitrocellulose membranes. After transfer, nitrocellulose membranes were cut into strips according to the molecular weights of the target proteins, including β-actin, when the proteins had clearly distinguishable sizes. This allowed each strip to be incubated with the appropriate primary and secondary antibodies within the same assay. Nitrocellulose membrane strips were blocked with 5% nonfat milk for 1 hour at room temperature and then incubated with respective primary antibodies, including anti-P2X7 (1: 500, sc-514962, Santa Cruz Biotechnology, CA, USA), anti-NLRP3 (1: 1000, SC06-23, Thermo Fisher Scientific, MA, USA), anti-TNF-α (1: 1000, ab205587, Abcam, MA, USA), anti-IL-1β (1: 2000, ab254360, Abcam), anti-IL-6 (1: 1000, ab259341, Abcam), anti-PPAR-γ (1: 1000, ab209350, Abcam), and anti-β-actin (1: 1000; sc47778, Santa Cruz Biotechnology) at 4 °C overnight. On the following day, the membrane strips were incubated with the corresponding HPR-conjugated secondary antibodies (1: 5000, Santa Cruz Biotechnology, Dallas, TX, USA) for 1 hour at room temperature. Immunoblot bands were further probed with a chemiluminescence reagent kit (ECL Plus; GE Healthcare). Because target proteins differed in abundance and exposure requirements, some target protein required longer exposure times, which could result in overexposure of β-actin or other highly abundant proteins. To address this, membrane strips of proteins with similar exposure requirements (from different gels, clearly labeled with gel numbers and sample identifiers) were developed together in the same exposure chamber. This approach was used for practical and technical optimization purposes.

Band intensities of target proteins, including loading control β-actin, were quantified using Image J software. Briefly, blot images were opened in ImageJ, and a rectangular region of interest was defined around the largest band of the target protein, along with an adjacent background region. The same region of interest dimensions were applied consistently to all bands within the same blot. Integrated density values were recorded for each band and exported to Excel, with lanes labeled according to sample ID. Inverted pixel density values were calculated for all data, and background values were subtracted to obtain background-corrected net values. β-Actin was used as an internal loading control, and the densitometric values of target proteins bands were normalized to that of corresponding β-actin bands. Six animals per group were included for densitometric analysis. Control and BD samples (1 sample/mouse and n=6 mice/group) were loaded in paired fashion (1 control followed by 1 BD sample, a total of 12 mice samples) and repeated across the same gel, transfer, and exposure conditions, thereby minimizing technical variability and ensuring consistent exposure and contrast between groups.

The antibodies used in this study were commercially validated antibodies widely used in prior peer-reviewed publications investigating inflammatory signaling pathways. Manufacturer-recommended conditions were followed, and preliminary experiments were performed to optimize the respective antibody dilution. To minimize potential confounding variables affecting cardiac function, physiologic conditions were standardized across all experimental groups. All animals underwent

Indexed in: [Science Citation Index Expanded] [Index Medicus/MEDLINE] [Chemical Abstracts] [Scopus]

Table 1. Phase I baseline characteristics.

	Control (n=8)	Brain death (n=10)	*P* value
Weight (g)	28.63±3.46	28.60±2.27	0.986
Temperature (˚C)	32.89±0.75	32.88±0.63	0.977
LV aread (mm^2)	15.66±4.00	18.63±3.99	0.138
LV areas (mm^2)	9.00±2.09	10.75±2.79	0.160
CO (mL/min)	8.52±1.70	9.88±1.86	0.155
LVEF (%)	63.3±4.93	59.4±5.92	0.164
FS (%)	16.1±4.70	19.7±5.25	0.153
SV (µL)	24.7±5.07	25.7±3.21	0.692
Vold (µL)	41.1±11.8	42.3±9.80	0.852
Vols (µL)	15.3±5.31	16.8±8.20	0.714
Heart rate (bpm)	389±48.5	366±37.4	0.298

Data are reported as mean±standard deviation. $area_d$, – area in diastole; $area_s$ – area in systole; CO – cardiac output; LV – left ventricle; LVEF – left ventricular ejection fraction; FS – fractional shortening; SV – stroke volume.

identical anesthetic induction and maintenance with isoflurane, temperature control using a heating pad and lamp, and continuous monitoring of electrocardiogram, electroencephalogram, and respiratory parameters. Mechanical ventilation settings, fluid supplementation, and laboratory monitoring were applied uniformly to both the control and BD groups. Baseline echocardiographic measurements confirmed physiologic equivalence between groups prior to experimental intervention. Western blot sample preparation, band detection, and densitometric analysis were performed by an investigator who was blinded to the experimental group assignment. Echocardiography was performed by a separate investigator using a standard acquisition protocol.

Statistical Analysis

Normality was assessed by Shapiro-Wilk tests and assessment of histograms and Q-Q plots. Homogeneity of variances was assessed with the Levene test. Independent-sample *t* tests were used to compare group means at each time point. One-way repeated measures analysis of variance (ANOVA) with post hoc pairwise comparisons and Bonferroni adjustment was used to assess intragroup differences in ejection fraction over time. Sphericity was confirmed with Mauchly's test. No log transformations were required. Data are presented as mean±standard deviation. A *P* value less than 0.05 was considered statistically significant. Animals that died during the experiment contributed data up to the time of death; missing values after death were not imputed.

Results

Phase I

Baseline characteristics between the 2 groups were equivalent (**Table 1**). Compared with animals in the control group, all animals in the BD group developed significantly depressed LVEF by T60 (BD 44.06±9.81% vs control 65.8±4.91%; *P*<0.001), and mean BD LVEF values were lower at T60 than at baseline (44.06±9.81% vs 59.44±5.92%; *P*=0.004), while mean LVEF for controls were similar (65.8±4.91% vs 63.25±4.93%; *P*=NS) (**Figure 2**). There were no deaths within 60 minutes. Blood gas and laboratory values were equivalent between groups. Six animals in each group survived to T120, while 4 of the total cohort survived to T180 (1 BD, 3 control). The number of animals analyzed at each time point is shown in **Figure 2**. Animals that died during the extended observation period contributed data to analyses at time points obtained prior to death but were not included in analyses for subsequent time points. Given that 100% of the animals in the BD group showed a statistically significant decline in LV systolic function by 60 minutes, and there was no attrition, we chose this time-point to study NLRP3-related inflammatory signaling in phase II.

Phase II

Baseline characteristics between the 2 groups were equivalent (**Table 2**). There was no attrition in phase II of the experiment. At T60, mean LVEF (BD 43.5±5.5% vs control 66.6±2.9%;

Indexed in: [Science Citation Index Expanded] [Index Medicus/MEDLINE] [Chemical Abstracts] [Scopus]

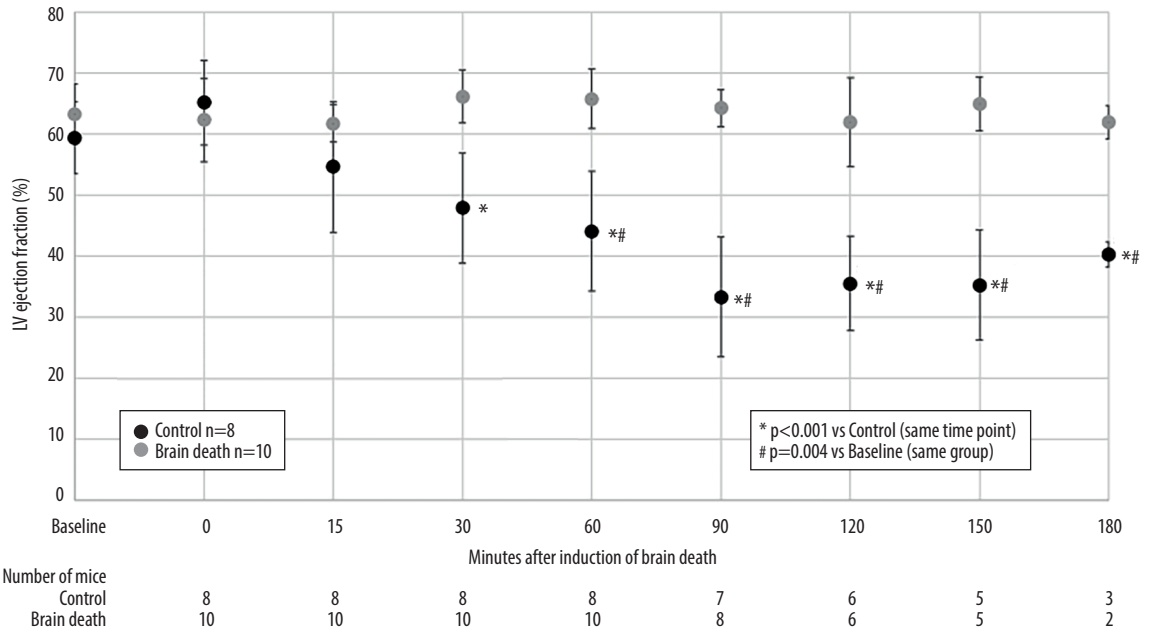

Figure 2. Phase I time-course of brain death induced systolic ventricular dysfunction in the murine left ventricle.

Table 2. Phase 2 baseline characteristics.

	Control (n=6)	Brain death (n=6)	*P* value
Weight (g)	27.7±2.9	27.3±3.0	0.819
Temperature (°C)	33.0±1.0	33.1±0.7	0.845
LV aread (mm^2)	17.3±5.3	17.5±2.6	0.936
LV areas (mm^2)	9.3±3.1	9.9±2.3	0.711
CO (mL/min)	9.2±2.5	9.2±1.8	1.00
LVEF (%)	63.2±8.9	62.6±3.9	0.883
FS (%)	14.5±2.9	16.8±3.4	0.236
SV (µL)	25.9±12.9	25.7±3.2	0.971
Vold (µL)	40.5±17.8	43.3±8.8	0.737
Vols (µL)	16.4±15.3	17.8±9.1	0.811
Heart rate (bpm)	414±69.5	358±54.3	0.159

Data are reported as mean±standard deviation. $area_d$ – area in diastole; $area_s$ – area in systole; CO – cardiac output; LV – left ventricle; LVEF – left ventricular ejection fraction; FS – fractional shortening; SV – stroke volume.

P<0.001) (**Figure 3**), fractional shortening (BD 14.2±4.9% vs control 20.1±4.0%; *P*=0.045), and stroke volume (BD 10.9±2.5 µL vs control 18.4±3.7 µL; *P*=0.002) were all significantly diminished in the BD group (**Table 3**). The BD group expressed higher NLRP3 (BD 1.47±0.26 vs control 1±0.31; *P*=0.019; **Figure 4A, 4B**) and IL-1β (BD 1.45±0.25 vs control 1±0.43; *P*=0.048; **Figure 4A, 4C**) in LV tissue than the control group. Proinflammatory cytokine expressions of TNF-α (BD 2.35±1.13 vs control 1±0.33; *P*=0.02; **Figure 4A, 4D**) and IL-6 (BD 2.48±1.06 vs control 1±0.70; *P*=0.03; **Figure 4A, 4E**) were also significantly greater in the BD group. LV P2X7 expression did not significantly differ between the 2 groups (**Figure 5A, 5B**), while there was a trend toward increased PPAR-γ in BD animals compared with the controls (BD 1.26±0.24 vs control 1±0.29; *P*=0.064; **Figure 5A, 5C**).

Indexed in: [Science Citation Index Expanded] [Index Medicus/MEDLINE] [Chemical Abstracts] [Scopus]

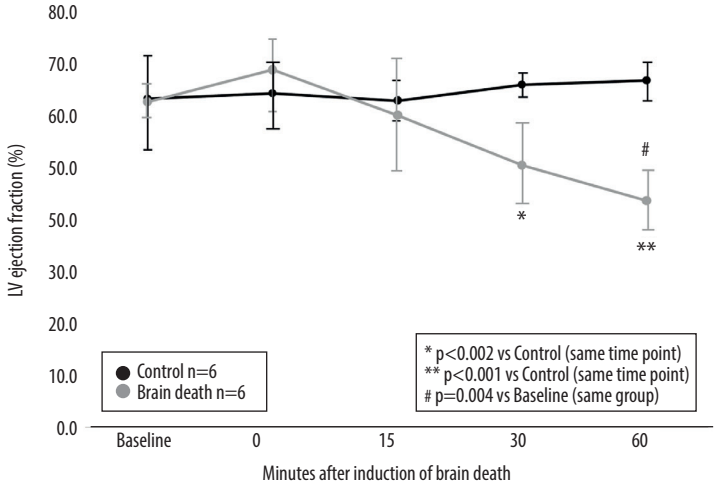

Figure 3. Phase II impact of brain death on systolic ventricular function in the murine left ventricle.

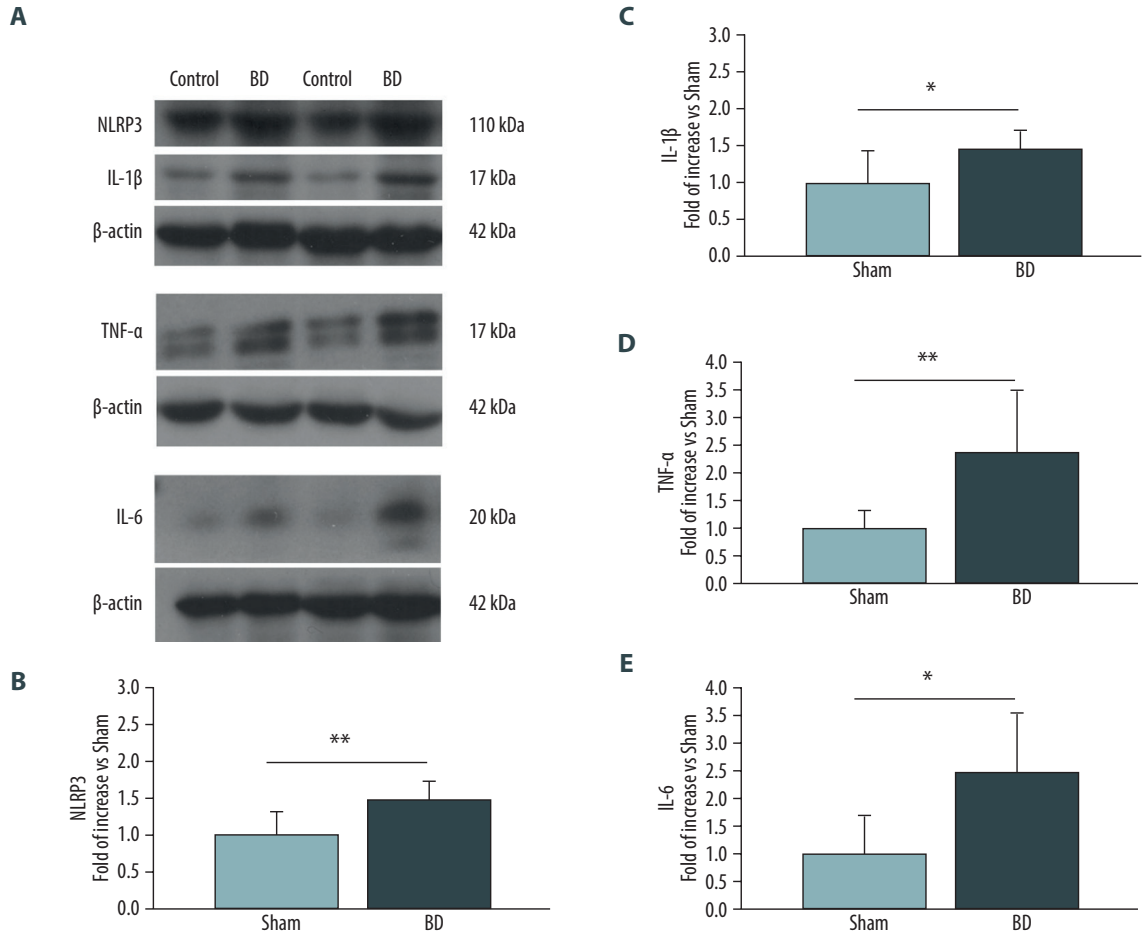

Figure 4. Phase II levels of NLRP3 and pro-inflammatory cytokines in left ventricle at 60 minutes after brain death (BD). (**A**) Representative western blot bands from 2 independent animal sets; (**B-E**) Quantitative analysis of NLRP3, IL-1β, TNF-α, and IL-6 expressions. n=6/group. ** *P*<0.01, * *P*<0.05 vs control.

Indexed in: [Science Citation Index Expanded] [Index Medicus/MEDLINE] [Chemical Abstracts] [Scopus]

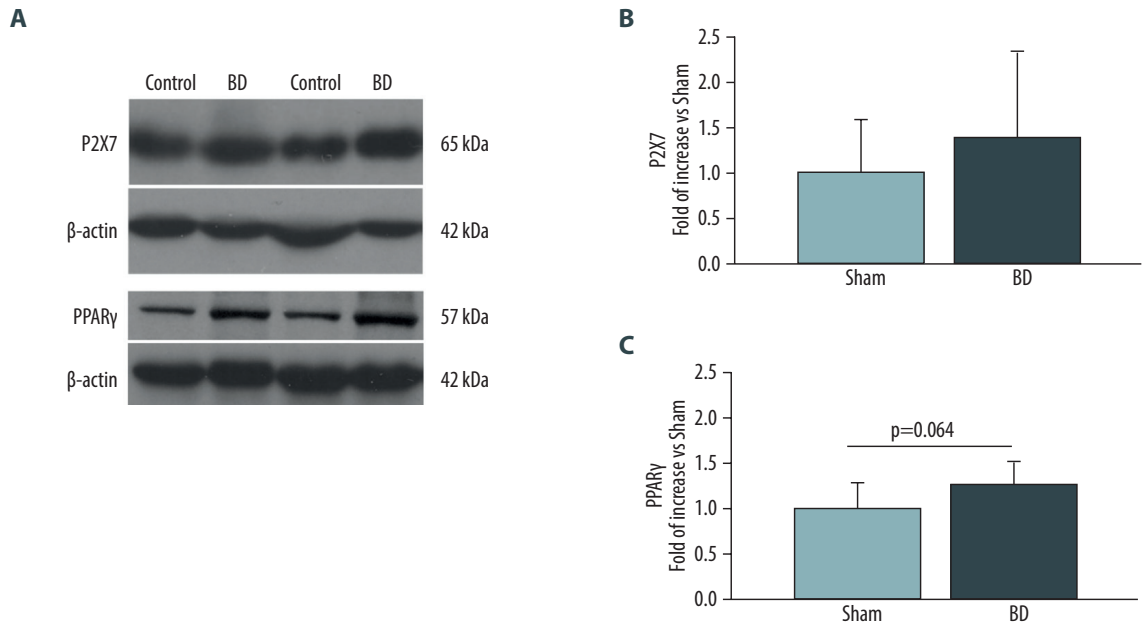

Figure 5. Phase II levels of P2X7 and PPAR-gamma in left ventricle at 60 minutes after brain death (BD). (**A**) Representative western blot bands from 2 independent animal sets (loading control β-actin band for PPAR-γ is the same as that used for NLRP3 and IL-1β in Figure 4A, as these proteins were probed on the same membrane). (**B, C**) Quantitative analysis of P2X7 and PPAR-gamma expressions. n=6/group.

Discussion

We used a previously validated and well-established model of brain death [15-17], mimicking the rise in intracerebral pressure that accompanies traumatic brain injury or hemorrhagic cerebral vascular accident, common mechanisms of brain death in the potential organ donor population, to demonstrate several important findings. In phase I, we showed that in this mouse model, the incidence of brain death induced systolic ventricular dysfunction in the left ventricle was 100% at 60 minutes. Baseline ejection fraction in the murine LV dropped from 60% to 65%, to 40% to 45% in the BD group at 60 minutes and then hovered between 30% and 40% for the duration of 180 minutes. Although there were no deaths at 60 minutes, there was a significant attrition by 2 hours (25% in control group and 40% in BD group). In phase II of the study, the decrease in LV function in the BD group was associated with increased levels of NLRP3 and inflammatory cytokines, including IL-1β, TNF-α, and IL-6, in the LV tissues. There was also a tendency of increased PPAR-γ in the LV tissue in the BD group. Brain death causes acute and massive catecholamine release, leading to an inflammatory state characterized by cytokine upregulation [4,18]. Accumulating evidence suggests that brain death–induced inflammatory activity adversely affects graft survival [4,19] and is associated with reduced heart contractile function in sheep [5]. Consistent with those results, higher cytokine levels in LV tissue and reduced LV function were found in the current mouse model of BD, suggesting that this model may serve as a reliable platform for studying myocardial dysfunction induced by brain death.

Prior experimental studies in large-animal and rodent models have demonstrated that brain death is associated with myocardial inflammation and impaired cardiac contractility. For example, Walweel et al reported increased proinflammatory cytokine production and reduced cardiac function in a sheep model of brain death [5], while other murine brain-death models have demonstrated inflammatory immune activation and complement-mediated myocardial injury [16,17]. Our findings are consistent with these observations and expand on prior work by demonstrating a reproducible time course of systolic ventricular dysfunction using echocardiographic assessment and by identifying an association between ventricular dysfunction and increased expression of NLRP3-related inflammatory signaling components in LV tissue. To the best of our knowledge, the association between brain death–induced ventricular dysfunction and myocardial NLRP3-related inflammatory signaling has not been previously described in a murine model.

NLRP3 expression has been observed not only in leucocytes but also in cells of the cardiovascular system, such as vascular endothelial cells, vascular smooth muscle cells, and cardiomyocytes [20]. NLRP3 inflammasomes are intracellular inflammatory machinery that mediate production of IL-1β, a

Indexed in: [Science Citation Index Expanded] [Index Medicus/MEDLINE] [Chemical Abstracts] [Scopus]

Table 3. Impact of brain death on ventricular mechanics over time (T), at 0, 15, 30, and 60 minutes.

	T0	T15	T30	T60
Temperature (˚C)				
Control	32.5±0.8	32.7±0.4	33.2±1.2	33.5±0.7
Brain death	33.1±0.6	32.6±0.8	32.4±0.9	32.3±0.8
P value	0.172	0.790	0.221	0.172
Aread (mm^2)				
Control	15.3±2.9	14.9±2.6	13.9±1.9	13.7±2.0
Brain death	13.8±1.8	12.5±1.7	12.3±1.3	12.1±1.2
P value*	0.307	0.088	0.120	0.124
Areas (mm^2)				
Control	8.1±1.9	8.0±1.6	7.2±1.2	7.0±1.2
Brain death	6.9±1.5	7.0±1.7	7.4±1.6	7.9±1.1
P value*	0.253	0.319	0.811	0.069
CO (mL/min)				
Control	9.5±3.0	7.4±2.6	6.8±2.5	6.9±2.7
Brain death	9.4±2.6	7.3±2.4	5.9±1.9	5.2±1.9
P value*	0.268	0.946	0.499	0.236
LVEF (%)				
Control	64.2±8.1	62.8±4.4	65.9±5.0	66.6±2.9
Brain death	68.7±6.1	59.9±9.9	50.4±7.2	43.5±5.5
P value*	0.303	0.527	0.002	0.001
FS (%)				
Control	18.1±2.8	17.1±2.9	20.0±4.7	20.1±4.0
Brain death	22.6±4.8	18.9±7.4	15.9±5.5	14.2±4.9
P value*	0.075	0.591	0.195	0.045
SV (µL)				
Control	21.1±6.2	20.0±4.9	18.8±3.3	18.4±3.7
Brain death	19.6±2.8	15.7±1.4	12.5±1.9	10.9±2.5
P value*	0.601	0.066	0.002	0.002
Vold (µL)				
Control	33.1±9.1	31.8±8.0	28.7±5.3	27.9±6.1
Brain death	30.4±5.3	26.2±4.6	23.9±4.6	23.8±4.8
P value*	0.544	0.168	0.125	0.225
HR (bpm)				
Control	405±77	406±57	420±53	430±47
Brain death	469±57	437±66	401±73	384±110
P value*	0.159	0.421	0.639	0.375

Data are reported as mean±standard deviation. aread – area in diastole; areas – area in systole; CO – cardiac output; LVEF – left ventricular ejection fraction; FS – fractional shortening; SV – stroke volume. * P value between groups at same time point.

Indexed in: [Science Citation Index Expanded] [Index Medicus/MEDLINE] [Chemical Abstracts] [Scopus]

proinflammatory cytokine, in response to exogenous and endogenous danger signals [21]. In our study, the LV tissue concentration of NLRP3 and proinflammatory cytokines IL-1β, IL-6, and TNF-α were increased at 1 hour after brain death, suggesting a potential role for NLRP3-related inflammatory signaling in myocardial dysfunction after brain death.

Upstream signaling potentially involved in the NLRP3 amplification was also investigated. P2X7 receptors, activated by extracellular ATP released from damaged cells, are highly expressed in immune cells, cardiac smooth muscle cells, and endothelial cells [22]. In the context of cardiac transplantation, P2X7 receptor expression was found to be upregulated in graft-infiltrating lymphocytes in cardiac-transplanted humans and mice [23]. Recent studies demonstrated that P2X7 could modulate the assembly of the NLRP3 inflammasome, leading to the secretion of proinflammatory factors and worsened cardiac disease phenotypes [24]. Most importantly, Higashikuni et al demonstrated that cardiac inflammation and myocardial hypertrophy were regulated by heart-brain interactions [10]. The depletion of ATP release from sympathetic efferent nerves, ablation of cardiac afferent nerves, or a lipophilic β-blocker was shown to reduce cardiac extracellular ATP levels and inhibit NLRP3 inflammasome activation and IL-1β production in mice [10]. In the present study, the protein level of P2X7 receptors was not significantly elevated in the LV tissue after BD. However, this may not preclude functionally meaningful changes in P2X7 activity, and P2X7 over-activation may contribute to downstream NLRP3-related inflammatory signaling. Future studies that directly assess P2X7 activity [21] and evaluate the effects of P2X7 inhibitors will help clarify whether neural signals after brain death contribute to myocardial dysfunction via an ATP/P2X7/NLRP3 axis.

PPAR-γ plays an anti-inflammatory role by inhibiting NF-κB activation and NLRP3-dependent IL-1β and IL-18 production [11]. By interacting with the NLRP3 inflammasome, PPAR-γ reduces NLRP3 inflammasome formation by interfering with NLRP3-NLRP3 interactions and NLRP3-dependent adaptor protein recruitments/oligomerization [11]. In the present study, the slight increase in endogenous PPAR-γ expression at 1 hour after brain death was not accompanied by reduced levels of NLRP3 and proinflammatory cytokines. Nevertheless, PPARγ participates in anti-oxidant and anti-apoptosis signaling in addition to having anti-inflammatory effects [25]. Previous work has shown that cardiomyocyte-specific overexpression of PPARγ prevented cardiac dysfunction in an lipopolysaccharide-induced sepsis model without significant reduction in early myocardial inflammatory gene expression, including IL-1β, IL-6, and TNF-α, suggesting that functional protection may be mediated by a mechanism other than early inflammatory suppression [26]. Whether the observed change of PPARγ reflects an endogenous cardioprotective response to BD remains unclear.

From a translational perspective, modulation of inflammatory signaling in the brain-dead donor represents a potential strategy for preserving donor heart function prior to transplantation. Pharmacologic inhibition of the P2X7 receptor has been shown to attenuate inflammatory responses in cardiovascular disease models, while PPAR-γ agonists are already clinically available and have demonstrated anti-inflammatory effects in experimental systems [12,13]. Although the present study did not demonstrate significant changes in endogenous P2X7 expression and only a trend toward increased PPAR-γ expression in LV tissue, these pathways remain biologically plausible therapeutic targets for mitigating brain death-induced myocardial dysfunction. Future studies evaluating pharmacologic modulation of these pathways in donor management models may help determine their clinical relevance.

There are limitations of this study. First, there was significant attrition by 2 hours (25% and 40% in the control and BD groups, respectively) in the mouse model, for which we do not have a definitive explanation, and which may have introduced survivorship bias in estimates at later phase I time points (t=120-180). Possibilities may be inadequate fluid supplementation for a 3-hour procedure, high physiologic stress during imaging, and/or the continuous 0.9% to 1% isoflurane anesthesia in the setting of brain death (in the BD group) to prevent confounding effects on the murine cardiovascular physiology. Second, sex effects were not evaluated. Third, our results suggested a strong association between NLRP3-related inflammation and LV dysfunction, but the design of our study does not prove causation. It is possible an unmeasured factor resulted in increased inflammation and LV dysfunction. Since NLRP3 inflammasome activation (eg, caspase-1 activation or ASC oligomerization) were not measured directly, conclusions regarding inflammasome involvement are based on protein expression and cytokine associations rather than functional activation assays. Fourth, despite standardized physiologic management, residual confounding related to anesthetic exposure, mechanical ventilation, fluid balance, and procedural stress cannot be completely excluded from the model. Finally, phase II of our experiment included 6 animals per group, which was chosen to satisfy ethical principles of reduction in animal research [27]; however, the small sample substantially limits statistical power for detecting differences in protein expression and inflammatory markers. This limitation is particularly relevant for conclusions regarding upstream regulators, such as P2X7 and PPAR- γ, where non-significant results may reflect insufficient power rather than an absence of biological effect.

Conclusions

In conclusion, there was systolic LV dysfunction in the murine model of BD, with 100% incidence at 60 minutes prior to the

Indexed in: [Science Citation Index Expanded] [Index Medicus/MEDLINE] [Chemical Abstracts] [Scopus]

onset of any attrition. The BD-induced LV dysfunction was associated with increased tissue expressions of NLRP3 and inflammatory cytokines in LV tissues. Further exploration into the upstream signaling pathways involving the P2X7 receptor and/or PPAR-γ in NLRP3-related inflammatory signaling may hold promise as potential therapeutic strategies for preserving myocardial function after brain death.

Acknowledgements

The authors acknowledge Joshua S. Chung, MD, Anees J. Razzouk, MD, Khouloud Nasser, Jason Gatling, MD, Arlin Blood, MD, Lubo Zhang, MD, PhD, Ciprian Gheorge, MD, and John Zhang, MD, PhD.

Declaration of Figures' Authenticity

All figures submitted have been created by the authors who confirm that the images are original with no duplication and have not been previously published in whole or in part.

References:

1 Tryon D, Hasaniya NW, Bailey LL, et al. Effect of left ventricular dysfunction on utilization of donor hearts. J Heart Lung Transpl. 2018;37(3):349-57
2. Sibona A, Khush KK, Oyoyo UE, et al. Long-term transplant outcomes of donor hearts with left ventricular dysfunction. J Thorac Cardiovasc Surg. 2019;157(5):1865-75
3. Chen CW, Sprys MH, Gaffey AC, et al. Low ejection fraction in donor hearts is not directly associated with increased recipient mortality. J Heart Lung Transpl. 2017;36:611-15
4. Schwarz P, Custódio G, Rheinheimer J, et al. Brain death-induced inflammatory activity is similar to sepsis-induced cytokine release. Cell Transplant. 2018: 27(10):1417-24
5. Walweel K, Boon AC, See Hoe LE, et al. Brain stem death induces pro-inflammatory cytokine production and cardiac dysfunction in a sheep model. Biomed J. 2022;45(5):776-87
6. Wang Z, Hu W, Lu C, et al. Targeting NLRP3 (Nucleotide-binding domain, leucine-rich-containing family, pyrin domain-containing-3) inflammasome in cardiovascular disorders. Arterioscler Throm Vasc Biol. 2018;38(12):2765-79
7. Toldo S, Mezzaroma E, Buckley LF, et al. Targeting the NLRP3 inflammasome in cardiovascular diseases. Pharmacol Ther. 2022;236:108053
8. Mauro Ag, Bonaventura A, Mezzaroma E, et al. NLRP3 Inflammasome in acute myocardial infarction. J Cardiovasc Pharmacol. 2019;74(3):175-87
9. Pelegrin P. P2X7 receptor and the NLRP3 inflammasome: Partners in crime. Biochem Pharmacol. 2021;187:114385
10. Higashikuni Y, Liu W, Numata G, et al. NLRP3 inflammasome activation through heart-brain interaction initiates cardiac inflammation and hypertrophy during pressure overload. Circulation. 2023;147(4):338-55
11. Yang CC, Wu CH, Lin TC, et al. Inhibitory effect of PPAR-gamma on NLRP3 inflammasome activation. Theranostics. 2021;11(5):2424-41
12. Müller CE, Namasivayam V. Agonists, antagonists, and modulators of P2X7 receptors. Methods Mol Biol. 2022;2510:31-52
13. Landreth G, Jiang Q, Mandrekar S, Heneka M. PPAR-γ agonists as therapeutics for the treatment of Alzheimer's disease. Neurotherapeutics. 2008;5(3):481-89
14. National Academies of Sciences, Engineering, and Medicine. 2011. Guide for the Care and Use of Laboratory Animals: Eighth Edition. Washington, DC: The National Academies Press. https://doi.org/10.17226/12910
15. Pomper G, Trescher K, Santer D, et al. Introducing a mouse model of brain death. J Neurosci Methods. 2010;192(1):70-74
16. Floerchinger B, Yuan X, Jurisch A, et al. Inflammatory immune responses in a reproducible mouse brain death model. Transpl Immun. 2012;27(1):25-29
17. Atkinson C, Varela JC, Tomlinson S. Complement dependent inflammation and injury in a murine model of brain-dead donor hearts. Circ Res. 2009;105(11):1094-101
18. Santana AC, Andraus W, Zimelewicz Oberman D, et al. Immunomodulatory response in an experimental model of brain death. Sci Rep. 2023;13:10524
19. Watts RP, Thom O, Fraser JF. Inflammatory signaling associated with brain dead organ donation: From brain injury to brain stem death and posttransplant ischemia reperfusion injury. J Transplant. 2013;2013:521369
20. Zheng Y, Xu L, Dong N, Li F. NLRP3 inflammasome: The rising star in cardiovascular diseases. Front Cardiovasc Med. 2022;9:927061
21. Paik S, Kim JK, Silwal P, et al. An update on the regulatory mechanisms of NLRP3 inflammasome activation. Cell Mol Immunol. 2021;18(5):1141-60
22. Zhou J, Zhou Z, Liu X, et al. P2X7 receptor-mediated inflammation in cardiovascular disease. Front Pharmacol. 2021;12:654425
23. Vergani A, Tezza S, D'Addio F, et al. Long-term heart transplant survival by targeting the ionotropic purinergic receptor P2X7. Circulation. 2013;127(4):463-75
24. Guerra Martinez C. P2X7 receptor in cardiovascular disease: The heart side. Clin Exp Pharmacol Physiol. 2019;46:513-26
25. Ivanova EA, Parolari A, Myasoedova V, et al. Peroxisome proliferator-activated receptor (PPAR) gama in cardiovascular disorders and cardiovascular surgery. J Cardiol. 2015;66(4):271-78
26. Drosatos K, Khan RS, Trent CM. et al. PPARγ activation prevents sepsis-related cardiac dysfunction and mortality in mice. Circ Heart Fail. 2013;6(3):550-62
27. Russell WMS, Burch RL. The principles of humane experimental technique. 1959. Methuen, London

Indexed in: [Science Citation Index Expanded] [Index Medicus/MEDLINE] [Chemical Abstracts] [Scopus]